

# Understanding Representation Quality in Self-Supervised Models

Neha Kalibhat<sup>\*1</sup>, Kanika Narang<sup>2</sup>, Hamed Firooz<sup>2</sup>, Maziar Sanjabi<sup>2</sup>, Soheil Feizi<sup>1</sup>

<sup>1</sup>Department of Computer Science, University of Maryland - College Park

<sup>2</sup>Meta AI

## Abstract

Self-supervised learning has shown impressive results in downstream classification tasks. However, there is limited work in understanding their failure modes and interpreting their learned representations. In this paper, we study the representation space of six state-of-the-art self-supervised models including SimCLR, SwaV, MoCo, BYOL, DINO and SimSiam. Without the use of class label information, we discover highly activating features that correspond to unique physical attributes in images and exist mostly in correctly-classified representations. Using these features, we propose Self-Supervised Representation Quality Score (or *Q-Score*), a model-agnostic, unsupervised score that can reliably predict if a given sample is likely to be mis-classified during linear evaluation, achieving AUPRC of 91.45 on ImageNet-100 and 78.78 on ImageNet-1K. *Q-Score* can also be used as a regularization term on any self-supervised model to remedy low-quality representations through the course of pre-training. We show that pre-training with *Q-Score* regularization can boost the performance of six state-of-the-art self-supervised models on ImageNet-1K, ImageNet-100, CIFAR-10, CIFAR-100 and STL-10, showing an average relative increase of 1.8% top-1 accuracy on linear evaluation. On ImageNet-100, BYOL shows 7.2% relative improvement and on ImageNet-1K, SimCLR shows 4.7% relative improvement compared to their baselines. Finally, using gradient heatmaps and Salient ImageNet masks, we define a metric to quantify the interpretability of each representation. We show that highly activating features are strongly correlated to core attributes and enhancing these features through *Q-score* regularization improves the overall representation interpretability for all self-supervised models.

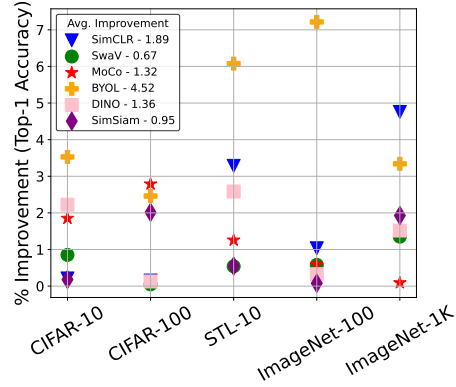


Figure 1. **Percentage improvement in top-1 accuracy on linear evaluation with *Q-Score* regularization:** In this figure, we show the percentage relative improvement in top-1 accuracy that we achieve when *Q-Score* regularization is used during pre-training on 5 datasets - CIFAR-10 [32], CIFAR-100 [33], STL-10 [16], ImageNet-100 [36] and ImageNet-1K [36], on 6 state-of-the-art self-supervised models - SimCLR [12], SwaV [10], MoCo [13], BYOL [24], DINO [11] and SimSiam [14]. In the legend, we show the average relative improvement for each model over 5 datasets. We observe that BYOL shows the highest relative improvement in accuracy on an average across 5 datasets. On ImageNet-1K we observe a maximum of 4.7% relative increase (on SimCLR) in top-1 accuracy.

## 1. Introduction

Self-supervised models learn to extract useful representations from data without relying on human supervision. These models [7, 10–14, 24, 29] have shown comparable results to supervised models in downstream classification tasks. By means of data augmentation, these models are trained to encode semantically relevant information from images while ignoring *nuisance* aspects. Therefore, the representations ultimately learned should only contain the information required to define a given sample. However, in practice, learned representations are often quite noisy and not interpretable, causing difficulties in understanding and

<sup>\*</sup>Correspondence to [nehamk@umd.edu](mailto:nehamk@umd.edu)

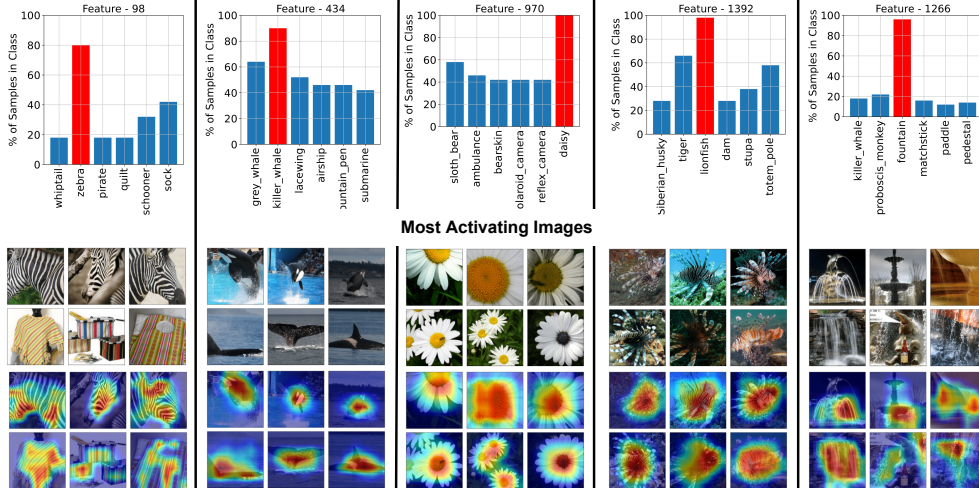


Figure 2. **Top activating images of various features:** In the top panel, we plot the percentage of samples (grouped by class) that are highly activated for each feature. We observe that these features show a strong correlation to one class or a group of classes. In the second panel, we observe the gradient heatmaps of the top activating samples for each feature. We observe that the heatmaps for a given feature, commonly highlight a unique physical characteristic which may be correlated to the ground truth of those images.

debugging their failure modes [21, 27, 28].

In this paper, our goal is to study the representation space of self-supervised models such as SimCLR [12], SwaV [10], MoCo [13], BYOL [24], SimSiam [14] and DINO [11] and discover their informative features in an unsupervised manner. This can help us debug models better, improve their representation spaces and make them more interpretable. To achieve these objectives, we visualize correct and mis-classified SimCLR representations of various ImageNet-1K classes as shown in Figure 3 (top panel). We observe that the representation space is very sparse: each representation contains a small number of features that are strongly deviated from the mean while the remaining features are close to zero in magnitude. We call these *highly activating features*. A similar observation has been made in recent works [28].

We observe some intriguing properties of highly activating features: (i) They may be highly activating for several samples in the population and therefore, can be strongly correlated to a particular class or group of classes (See Figure 2 top panel); (ii) They highlight useful/informative attributes in the activating samples (see Figure 2 bottom panel) which are often related to the ground truth of those samples; (iii) Although highly activating features are discovered without any label information, we observe that there are more such features in correctly classified representations than mis-classified representations (as shown in Figure 3).

Building on these observations, we propose a **sample-wise Self-Supervised Representation Quality Score (Q-Score)** that can be measured on a representation of any self-

supervised model (without requiring any label information). A high Q-Score for a sample implies that its representation contains highly activating features which is a favorable representation property. We empirically observe that Q-Score can be used as a predictor in distinguishing between correct and incorrect classifications by computing the Precision-Recall and ROC curves on 6 self-supervised models (Figure 4). Q-Score achieves 91.45 AUPRC (BYOL) and 73.26 AUROC (SimCLR) on ImageNet-100 and 78.78 AUPRC (BYOL) and 65.44 (SimCLR) on ImageNet-1K.

We next use Q-Score as a regularizer while pre-training self-supervised models to improve low-quality representations, pushing their representations to contain more highly activating features. We pre-train state-of-the-art self-supervised baselines from scratch with and without Q-Score regularization on CIFAR-10, CIFAR-100, STL-10, ImageNet-100 and ImageNet-1K. On an average (See Figure 1), across all experiments, Q-Score regularization improves the top-1 accuracy of linear evaluation by 1.8% (relative % change). On BYOL, we observe the highest relative increase of 7.2% on ImageNet-100 with Q-Score regularization. On ImageNet-1K, SimCLR shows the highest relative improvement of 4.7%. The representations, after regularization, show an improved structure, with more highly activating features as shown in Figure 3. We show that previously mis-classified are now classified correctly due to enhancement of their highly activating features.

Finally, we define a metric for quantifying representation interpretability by computing mean Intersection over Union (mIoU) with Salient ImageNet [38] masks used as ground truth. We show that, across all baselines, the highly activat-





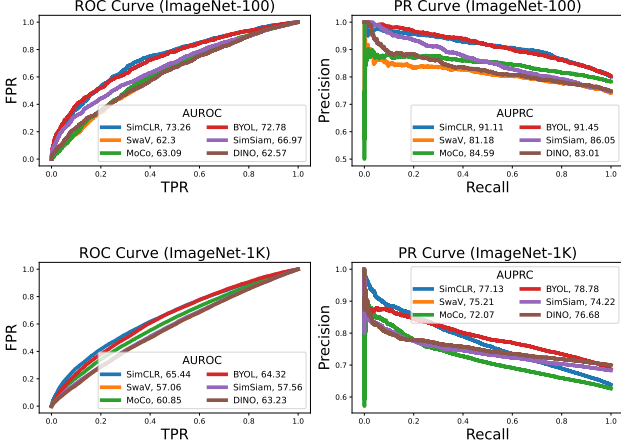


Figure 4. **Precision-Recall and ROC curves of Q-Score:** We compute the precision-recall and ROC curve of Q-Score for correct and mis-classified representations on ImageNet-100 and ImageNet-1K on SimCLR, SwaV, MoCo, BYOL, SimSiam and DINO. We achieve an AUPRC of up to 91.45 on ImageNet-100, 78.78 on ImageNet-1K and AUROC of 73.26 on ImageNet-100, 65.44 on ImageNet-1K when Q-score is used as a predictor in distinguishing between correct and mis-classified representations using Q-Score.

clustering techniques [3, 4, 8, 9, 18, 26, 44]. Self-supervised learning, is a recent approach to learn without human supervision by training models to prepare their own labels for each example [4, 17, 18, 42] usually with the help of a contrastive loss. Contrastive learning [1, 2, 40] usually uses a temperature-controlled cross-entropy loss between positive pairs of *similar* samples and negative pairs of *dissimilar* samples. Positive pairs are usually considered as multiple transformations (views) [39] of a given sample using stochastic data augmentation. Through this approach, several state-of-the-art self-supervised techniques [10, 12–14, 24, 29] have produced representations that show linear classification accuracy comparable to that of supervised approaches.

Understanding these learned representations is relatively less explored. [28], observes that self-supervised representations collapse to a lower dimensional space instead of the entire embedding space. Other methods [41, 43], propose to separate the representation space into variant and invariant information so that augmentations are not task-specific. [23] observes representations across layers of the encoder and compare it to supervised setups. Clustering-based or prototypical-based methods have also been proposed where the representation space is collapsed into a low-rank space [19, 30]. [5] uses an RCDM model to understand representation invariance to augmentations. [22] proposes a score based on the rank of all post-projector embed-

dings that can be used to judge and compare various self-supervised models.

In this work, we focus more on studying representations across correct and incorrect classifications in downstream classification tasks and understanding their properties (without using any labels). We investigate the connection between these unsupervised properties in the representation space and mis-classifications. Unlike [22] which requires computing rank over the entire dataset, our analysis leads to the development of an unsupervised *sample-wise* quality score which can be used as a regularizer and effectively improve downstream classification performance.

### 3. Highly Activating Features in Self-Supervised Representations

Let us consider a SimCLR model with a ResNet [25] base encoder  $f(\cdot)$  and an MLP projection head  $g(\cdot)$ . We define  $\mathbf{x}_i \in \mathbb{R}^n$  and  $\tilde{\mathbf{x}}_i \in \mathbb{R}^n$  as two transformed views of the  $i^{th}$  sample in a given input dataset containing  $N$  samples. We apply data transformations and pass the input samples through the base encoder to get self-supervised representations denoted by,  $f(\mathbf{x}_i) = \mathbf{h}_i \in \mathbb{R}^r$  and  $f(\tilde{\mathbf{x}}_i) = \tilde{\mathbf{h}}_i \in \mathbb{R}^r$ , where  $r$  is the size of the representation space. For contrastive training, we use the output of the projection head  $g(\mathbf{h}_i) = \mathbf{z}_i \in \mathbb{R}^p$  and  $g(\tilde{\mathbf{h}}_i) = \tilde{\mathbf{z}}_i \in \mathbb{R}^p$  where  $p$  is the size of the projection space. The SimCLR optimization for the set of model parameters  $\theta$ , is as follows,

$$\max_{\theta} \frac{1}{2N} \sum_{i=1}^{2N} \log \frac{\exp(\text{sim}(\mathbf{z}_i, \tilde{\mathbf{z}}_i))}{\sum_{j=1}^{2N} \mathbb{1}_{j \neq i} \exp(\text{sim}(\mathbf{z}_i, \mathbf{z}_j))} \quad (1)$$

where  $\text{sim}(\mathbf{z}_i, \mathbf{z}_j) = \frac{1}{\tau} \frac{\mathbf{z}_i^T \mathbf{z}_j}{\|\mathbf{z}_i\| \|\mathbf{z}_j\|}$ .

We now study some properties of representations that drive them to be correctly classified by a downstream linear classifier. In all our analysis, we perform L2 normalization over every representation vector  $\mathbf{h}$  to ensure fair comparison of features. In Figure 3, we visualize the representations ( $\mathbf{h}$ ) of SimCLR pre-trained on ImageNet-1K [36]. On the left, we show the average representations of correctly classified samples in a subset of classes, while on the right, we show the same for the mis-classified samples in those classes. There are 2048 columns corresponding to the number of features of a ResNet-50 [25] encoder, however, we display a small subset of those features for ease of visualization. The subset of features we display is the same for correct and incorrect classifications. The sample representations are illustrated in the form of heatmaps such that, features with higher magnitude show darker colors.

First, we study some visual properties of these representations. We observe that each representation is *nearly* sparse, i.e., most feature values are close to zero [28]. How-

ever, there exists a select few features that are strongly deviated from the remaining features in any given representation. For the  $i^{th}$  sample whose latent representation is  $\mathbf{h}_i \in \mathbb{R}^r$ , let  $\mu_i$  denote the mean of  $\mathbf{h}_i$  and  $\sigma_i$  denote the standard deviation of  $\mathbf{h}_i$ . We formally define the **set of highly activating features** ( $L_i$ ) for the  $i^{th}$  sample as,

$$L_i := \{j : h_{ij} > \mu_i + \epsilon\sigma_i\} \quad (2)$$

where  $\epsilon$  is a hyperparameter that is empirically selected. In practice, we find that  $\epsilon = 3$  works best for our experiments.

As we can see, in Figure 3, in the first panel, there is a clear difference between representations of correctly and incorrectly classified examples. Both correct and misclassified representations are *nearly* sparse, however, there are significantly more highly activating features in correct classifications. This is especially interesting because we can visually distinguish between correct and incorrect classifications, just by observing the highly activating features, without using any label information.

To further study the significance of highly activating features, we study the gradient heatmaps of their top activating samples (See Figure 2). We observe that the highly activating features of a sample may be unique to that particular sample or may be shared with other samples in the population. In Figure 2 (top panel), we plot all the samples where the given feature is highly activated (we call these highly activating samples for that feature) and group them by their class labels. Note that, the selection of highly activating features is done without using any label information. If we take feature 98, we observe that it is highly activated for over 80% of the "zebra" class which is significantly higher compared to that of remaining classes. In the bottom panel, we observe that the gradient heatmaps of the top activating samples of feature 98 correspond to "stripes", which is a meaningful physical attribute that is useful in identifying a "zebra" and can exist for other classes as well. Similarly, we plot the class distribution of features 434, 870, 1266 and 1392 to show that features correspond to some informative physical attributes which may be specific to a particular class or group of classes.

The correlation of highly activating features to unique physical attributes, suggests that their presence may be useful in correctly classifying representations. In Figure 3, our claim is confirmed as we observe that mis-classified representations do not show high activations on these features. Therefore, for any given sample, we can consider highly activating features as strong signals indicating classification outcome. We would like to emphasize that our results only indicate an *association* between these structural properties and classification accuracy and we do not claim any causal relationship between the two. In the next Sec-

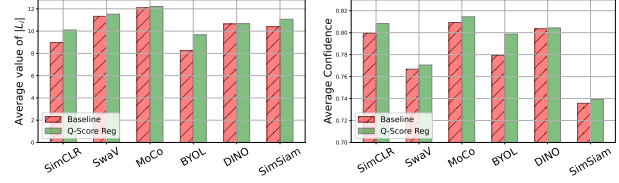


Figure 5. **Average  $|L_i|$  (left) and classification confidence (right) before and after regularization:** On the left we plot the average value of  $|L_i|$  (number of highly activating features) and on the right we plot the average classification confidence over the population of ImageNet-1K. We observe that both the number of highly activating features and classification confidence consistently improve on every self-supervised baseline with Q-Score regularization. This improvement is due to the nature of Q-Score regularization which maximizes highly activating features over the course of pre-training leading to a higher number of such features and improved classification confidence.

tion 4, we show that enhancing these properties, through regularization, improves the overall quality of representations, followed by improved classification accuracy and interpretability.

In the Appendix section A.1, we show that among the union of all highly activating features across all samples in the population, we can select a small subset of features called *discriminative features* that are relatively more informative and class-correlated. We show that with discriminative features, we can compress the representation space by up to 40% without affecting linear evaluation performance to a large extent. Since our analysis assumes that highly activating features are axis-aligned, we also perform a PCA analysis on the representation space (see Appendix Section A.2) to partially validate this assumption. We show that the gradient heatmaps of the highly activating features are strongly correlated with that of highly activating PCA features. Moreover, we show that discriminative features and PCA features perform comparably in downstream linear evaluation, up to 40% reduction in representation size.

## 4. Self-Supervised Representation Q-Score

In our study of learned representation patterns we observe that every representation contains a small number of highly activating features ( $L_i$ ) which are informative of physical concepts. Moreover, we observe that highly activating features are strong signals in distinguishing between correct and incorrect classifications. We combine these observations to design a sample-wise quality score for self-supervised representations.

Given, the representation of the  $i^{th}$  sample  $\mathbf{h}_i \in \mathbb{R}^r$ , we have defined the set of highly activating samples as  $L_i = \{j : h_{ij} > \mu_i + \epsilon\sigma_i\}, |L_i| < r$ , where,  $\mu_i$  is the mean of

$\mathbf{h}_i$ ) and  $\sigma_i$  is the standard deviation of  $\mathbf{h}_i$ . We define our Self-Supervised Representation Quality Score for sample  $i$  as,

$$Q_i := \frac{1}{|L_i|} \sum_{j \in L_i} (h_{ij} - \mu_i) \quad (3)$$

Intuitively, higher  $Q_i$  implies that the representation contains highly activated features which are strongly deviated from the mean. Our objective with this metric is to compute a sample-specific score in an unsupervised manner indicating the quality of its representations. Ideally, we would like to argue that samples with higher Q-score have improved representations and thus are more likely to be classified correctly in the downstream task. This is a general score that can be applied to any self-supervised model trained on any dataset. See Appendix Section A.3, for a discussion on Q-Score in supervised models.

Next, we measure how effective our score is in differentiating between correctly and incorrectly classified representations in an unsupervised manner. In Figure 4, we plot the Precision-Recall (PR) curve and the Receiver Operating Characteristic (ROC) curve of Q-Score when used as a predictor of classification outcome (correct or incorrect). We show this for SimCLR, SwaV, MoCo, BYOL, DINO and SimSiam for the validation set of ImageNet-100 containing 5000 samples (top panel) and ImageNet-1K containing 50000 samples (bottom panel). We also compute the AUROC (area under receiver operating characteristic curve) and AUPRC (area under precision-recall curve) of these curves. We observe AUPRC up to 91.45 on ImageNet-100 and 78.78 on ImageNet-1K on BYOL. On SimCLR, we observe AUROC up to 73.26 on ImageNet-100 and 65.44 on ImageNet-1K. Based on these results we can conclude that, Q-Score is a reliable metric in assessing the quality of representations, meaning that representations with lower Q-Score (quality), are more likely to be mis-classified.

We now check if promoting Q-Score during training is helpful. To do so, we use Q-Score as a regularizer while pre-training state-of-the-art self-supervised models. For example, we can apply this regularizer to the SimCLR optimization as follows,

$$\max_{\theta} \frac{1}{2N} \sum_{i=1}^{2N} \left[ \log \frac{\exp(\text{sim}(\mathbf{z}_i, \tilde{\mathbf{z}}_i))}{\sum_{j=1}^{2N} \mathbb{1}_{j \neq i} \exp(\text{sim}(\mathbf{z}_i, \mathbf{z}_j))} + \lambda \mathbb{1}_{Q_i < \alpha} (Q_i) \right] \quad (4)$$

where,  $\alpha$  is a threshold with which we select the low-score samples whose Q-Scores should be maximized and  $\lambda$  is the regularization coefficient. In other words the goal of this regularization is to improve low-quality representations, similar to the ones shown in Figure 3, by maximizing

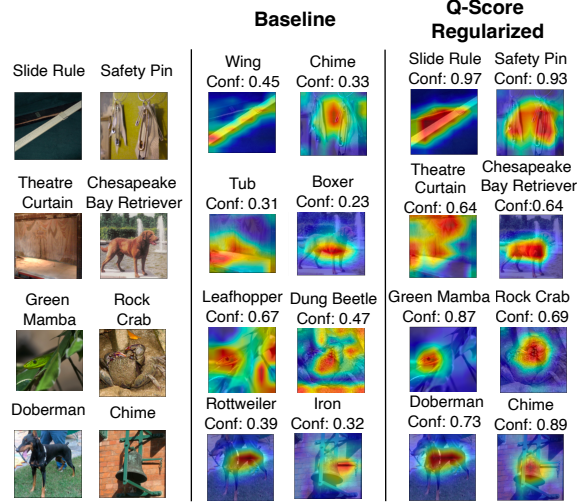


Figure 6. **Heatmaps of highly activating features of mis-classified samples:** We visualize the gradient heatmaps of the highly activating features of mis-classified images in the SimCLR ImageNet-1K baseline. We observe that the heatmaps before regularization activate portions that may not be relevant to the image ground truth, leading to incorrect predictions. After Q-Score regularization, the highly activating features show more localized, less noisy heatmaps. This improvement in quality leads to better classification with higher confidence.

their highly activating features for downstream classification.

#### 4.1. Experimental Setup

Our setup consists of state-of-the-art self-supervised encoders ( $f(\cdot)$ ) SimCLR [12], SwaV [10], MoCo [13], BYOL [24], DINO [11] (ResNet-based) and SimSiam [14] that we pre-train on datasets - ImageNet-1K [36], ImageNet-100 [36], CIFAR-10 [32], CIFAR-100 [33] and STL-10 [16]. We use a ResNet-50 encoder for our ImageNet-1K experiments and ResNet-18 encoder for all other datasets. We use a maximum of 4 NVIDIA RTX A4000 GPUs (16GB memory) for all our pre-training experiments. We maintain the same encoder optimizers and training parameters as the respective papers. For ImageNet experiments, due to our limited resource constraints, we use a batch size of 128 and pre-train for 100 epochs. We have tried to match our baseline numbers as much as possible within the error bars reported in the papers using the available resources. We pre-train each encoder on the self-supervised objective with and without Q-Score regularization (controlled by  $\lambda$ ). We perform standard linear evaluation by passing frozen pre-trained representations through a linear classifier that predicts class labels. For all our gradient heatmap visualizations, we utilize GradCAM [37].



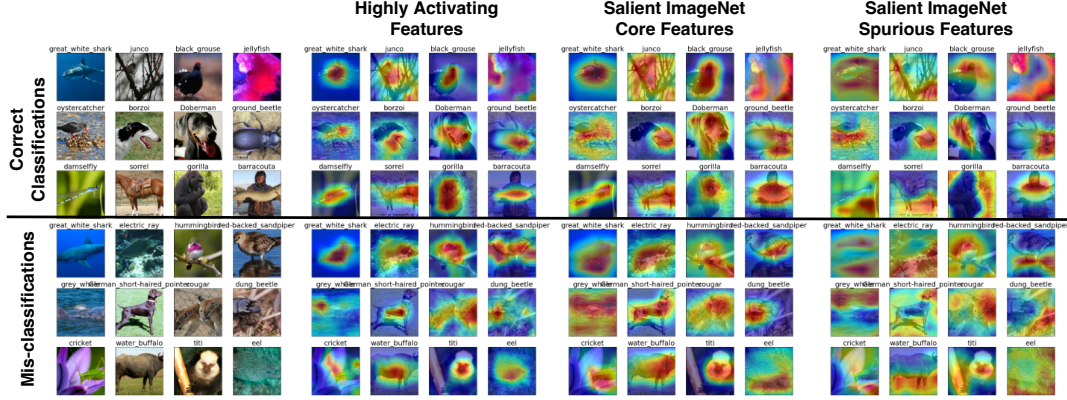


Figure 7. **Comparing highly activating features with Salient ImageNet *core* and *spurious* features:** We compare the gradient heatmaps of highly activating features correct and incorrect classifications of SimCLR on ImageNet-1K with the core and spurious masks of the same images in Salient ImageNet [38]. We observe that highly activating features generally overlap more with core features in Salient ImageNet.

## 4.2. Q-Score Regularization

We tabulate our results on pre-training various self-supervised baselines including SimCLR, SwaV, MoCo, BYOL, DINO and SimSiam with and without Q-Score regularization in Table 1. Q-Score regularization improves the top-1 accuracy on each dataset on all of the self-supervised state-of-the-art models. On ImageNet-100, we observe the most improvement on BYOL showing 7.2% relative increase in top-1 accuracy. On ImageNet-1K we observe a 4.7% relative improvement in accuracy on SimCLR. We summarize the relative improvements on all datasets and models in Figure 1. Q-Score is therefore a powerful regularizer that can boost the performance of state-of-the-art self-supervised baselines.

In addition to top-1 accuracy, Q-Score also shows significant improvement in representation quality. In Figure 3, we compare the representation space with and without Q-Score regularization. We observe that the number of highly activating features increases with Q-Score regularization on both correct and mis-classified representations. In Figure 5, we plot the mean of  $|L_i|$  (left), i.e., number of highly activating features in the  $i^{th}$  sample, and the mean linear classification confidence (right) over the population for each self-supervised model pre-trained with and without Q-Score regularization. We observe an increase in the average number of highly activating features ( $L_i$ ) and as a result, an improvement in classification confidence, due to more enhanced features. Our regularization produces better quality representations with clear highly activating features making them more distinguishable across classes and therefore, easier to classify. Due to this, we can attribute the improvement in performance to improved representation quality. Although Q-Score improves accuracy, it does not entirely prevent mis-classifications as mis-classifications may occur due to a variety of reasons such as, hardness of sam-

ples, encoder capacity, dataset imbalance etc.

Our motivation for using highly activating features as discussed in Section 3 is because - a) they are at clear contrast between correct and incorrect classifications, and b) they show strong correlation to ground truth in most cases. We observed in Figure 3 in the baseline, that the highly activating features in correctly classified samples are not as activated in mis-classified samples. We now study some mis-classified samples and observe how their features may improve with Q-Score regularization. In Figure 6, we visualize the gradient heatmaps of the highly activating features of some mis-classified examples in SimCLR. In the baseline, we observe that highly activating features do highlight portions of the image relevant to the ground truth, however, they may also activate other portions that are not necessarily important (see rock crab and green mamba). These heatmaps reflect low quality representations that do not contain features that are strongly deviated from the mean. After Q-Score regularization, the enhancement of highly activating features also leads to better gradient heatmaps that are more localized and cover almost all important portions of the image relevant to the ground truth. Therefore, these samples get classified correctly with higher confidence after regularization.

## 5. Quantifying Representation Interpretability with Salient ImageNet

We have observed that highly activating features in representations correspond to meaningful physical attributes through gradient heatmaps and they play a key role in deciding the downstream classification outcome. In this section, we quantify the interpretability of these features between correct and incorrect classifications. We utilize Salient ImageNet [38] as the ground truth baseline to compare our gradient heatmaps with. The Salient ImageNet dataset con-

tains annotated masks for both "core" and "spurious" features extracted from a supervised robust ResNet-50 model for 6858 images spanning 327 ImageNet classes. We also contains some text keywords, provided by workers to explain each feature. Core features are those that are highly correlated with the ground truth of the image, whereas, spurious features are those that activate portions irrelevant to the ground truth. In Figure 7, we study some correct and mis-classified samples in the SimCLR baseline. We plot the gradient heatmaps of the highly activating features (combining each individual feature heatmap) of SimCLR for each respective image. We also plot the core and spurious masks of the same images from the Salient ImageNet dataset. We observe that highly activating SimCLR features mostly capture relevant and defining characteristics of the images, therefore are highly correlated with the ground-truth. Moreover, for every correctly classified image, these heatmaps overlap more with core features than spurious features in Salient ImageNet. Highly activating features in mis-classified images also overlap with core features in most cases. Since highly activating features are very closely related (in terms of overlap) to *core* features, we can potentially explain these features better with the help of worker annotations in Salient ImageNet. Therefore, these features can be considered as *interpretable*.

We quantitatively measure the interpretability of a given representation of a given model by computing the Intersection over Union (mIoU) between the heatmap of highly activating features and the core or spurious mask of that image in Salient ImageNet. We can extend this to measure the overall interpretability of a given model by computing the mean Intersection over Union (mIoU) over the population. For the  $i^{th}$  image, we define  $Ar_i$  as the area of the heatmap of its highly activating features. Let  $Ar_i^{core}$  and  $Ar_i^{sp}$  be the area of the core and spurious masks respectively. The mIoU scores are defined as follows,

$$mIoU^{core} = \frac{1}{N} \sum_i \frac{s(Ar_i \cap Ar_i^{core})}{s(Ar_i \cup Ar_i^{core})}$$

$$mIoU^{sp} = \frac{1}{N} \sum_i \frac{s(Ar_i \cap Ar_i^{sp})}{s(Ar_i \cup Ar_i^{sp})}$$

where  $s(\cdot)$  calculates the sum of the pixel values of the highly activating features' heatmap in the given area. Higher  $mIoU^{core}\%$  indicates that, on an average higher percentage of the feature heatmap overlaps with the annotated core region, meaning that the model features are more interpretable.

In Table 8, we show that for all self-supervised baselines,  $mIoU^{core} > mIoU^{sp}$  for both correct and incorrect classifications which confirms that highly activating features generally encode important and core attributes over the whole

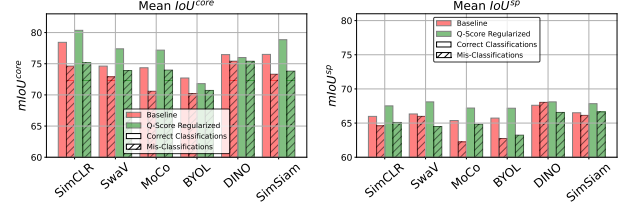


Figure 8. **mIoU scores with core and spurious Salient ImageNet features:** In the first plot, we compute the mean  $mIoU^{core}$  scores of 6 SSL baselines (using their highly activating features) before and after Q-Score regularization. In the second plot, we compute  $mIoU^{sp}$  in the same manner. We observe that highly activating features for all models generally show higher % IoU with core features than spurious features. Mis-classified representations show relatively lower % IoU with core features. After Q-score regularization, we observe that  $mIoU^{core}$  generally improves for both correct and mis-classified representations.

population. Among correct and mis-classified samples in the baselines, we observe that the  $mIoU^{core}$  of correct classifications is higher than mis-classifications. This aligns with our observations in Figure 6, which shows that highly activating features in mis-classified samples may not be strongly deviated from the mean and therefore, may correspond to less important portions of the image. After Q-Score regularization, we observe an increase in  $mIoU^{core}$  for both correct and mis-classified samples compared to the baseline. This shows that our regularization which enhances highly activating features produces better gradient heatmaps which are more overlapped with core portions of images and therefore, improves the overall model interpretability.

## 6. Conclusion

In this paper, we studied the representation space of self-supervised models and discovered that each representation contains a small number of highly activating features. These features can be correlated to classes or groups of classes and correspond to unique physical attributes. More importantly, correct classifications show significantly more highly activated features compared to mis-classified ones. Building on these observations, we define an unsupervised sample-wise score, Self-Supervised Representation Quality Score (Q-Score) that is effective in determining how likely samples are to be correctly or incorrectly classified. With the help of Q-Score regularization during pre-training, we remedied low-quality samples by improving their Q-Scores, thereby, improving the overall accuracy of state-of-the-art self-supervised models on ImageNet-1K by up to 4.7%. We also quantify representation interpretability with an IoU metric using Salient ImageNet masks as ground truth. With this metric, we confirm that highly activating features are more overlapped with core attributes. We also observed

that regularization improves over model interpretability due to enhancing highly activating features. Our paper poses important questions for future studies such as: 1) what are the causes of mis-classifications, apart from representation quality, 2) how can we better explain self-supervised features, given that there are no labels, 3) how can we utilize the better representations space for other tasks besides classification.

## References

- [1] Sanjeev Arora, Hrishikesh Khandeparkar, Mikhail Khodak, Orestis Plevrakis, and Nikunj Saunshi. A theoretical analysis of contrastive unsupervised representation learning, 2019. 4
- [2] Philip Bachman, R Devon Hjelm, and William Buchwalter. Learning representations by maximizing mutual information across views. In H. Wallach, H. Larochelle, A. Beygelzimer, F. d'Alché-Buc, E. Fox, and R. Garnett, editors, *Advances in Neural Information Processing Systems*, volume 32. Curran Associates, Inc., 2019. 4
- [3] Miguel A Bautista, Artsiom Sanakoyeu, Ekaterina Tikhoncheva, and Bjorn Ommer. Cliqecnn: Deep unsupervised exemplar learning. In D. Lee, M. Sugiyama, U. Luxburg, I. Guyon, and R. Garnett, editors, *Advances in Neural Information Processing Systems*, volume 29. Curran Associates, Inc., 2016. 4
- [4] Piotr Bojanowski and Armand Joulin. Unsupervised learning by predicting noise. In Doina Precup and Yee Whye Teh, editors, *Proceedings of the 34th International Conference on Machine Learning*, volume 70 of *Proceedings of Machine Learning Research*, pages 517–526. PMLR, 06–11 Aug 2017. 4
- [5] Florian Bordes, Randall Balestriero, and Pascal Vincent. High fidelity visualization of what your self-supervised representation knows about, 2021. 4
- [6] Lukas Bossard, Matthieu Guillaumin, and Luc Van Gool. Food-101 – mining discriminative components with random forests. In *European Conference on Computer Vision*, 2014. 13, 14
- [7] Mathilde Caron, Piotr Bojanowski, Armand Joulin, and Matthijs Douze. Deep clustering for unsupervised learning of visual features. *Lecture Notes in Computer Science*, page 139–156, 2018. 1
- [8] Mathilde Caron, Piotr Bojanowski, Armand Joulin, and Matthijs Douze. Deep clustering for unsupervised learning of visual features. In *Proceedings of the European Conference on Computer Vision (ECCV)*, September 2018. 4
- [9] Mathilde Caron, Piotr Bojanowski, Julien Mairal, and Armand Joulin. Unsupervised pre-training of image features on non-curated data. In *Proceedings of the IEEE/CVF International Conference on Computer Vision (ICCV)*, October 2019. 4
- [10] Mathilde Caron, Ishan Misra, Julien Mairal, Priya Goyal, Piotr Bojanowski, and Armand Joulin. Unsupervised learning of visual features by contrasting cluster assignments. In H. Larochelle, M. Ranzato, R. Hadsell, M. F. Balcan, and H. Lin, editors, *Advances in Neural Information Processing Systems*, volume 33, pages 9912–9924. Curran Associates, Inc., 2020. 1, 2, 3, 4, 6, 11
- [11] Mathilde Caron, Hugo Touvron, Ishan Misra, Hervé Jégou, Julien Mairal, Piotr Bojanowski, and Armand Joulin. Emerging properties in self-supervised vision transformers. In *Proceedings of the IEEE/CVF International Conference on Computer Vision (ICCV)*, pages 9650–9660, October 2021. 1, 2, 3, 6, 11
- [12] Ting Chen, Simon Kornblith, Mohammad Norouzi, and Geoffrey Hinton. A simple framework for contrastive learning of visual representations. In Hal Daumé III and Aarti Singh, editors, *Proceedings of the 37th International Conference on Machine Learning*, volume 119 of *Proceedings of Machine Learning Research*, pages 1597–1607. PMLR, 13–18 Jul 2020. 1, 2, 3, 4, 6, 11
- [13] Xinlei Chen, Haoqi Fan, Ross Girshick, and Kaiming He. Improved baselines with momentum contrastive learning, 2020. 1, 2, 3, 4, 6, 11
- [14] Xinlei Chen and Kaiming He. Exploring simple siamese representation learning. In *Proceedings of the IEEE/CVF Conference on Computer Vision and Pattern Recognition (CVPR)*, pages 15750–15758, June 2021. 1, 2, 3, 4, 6, 11
- [15] M. Cimpoi, S. Maji, I. Kokkinos, S. Mohamed, , and A. Vedaldi. Describing textures in the wild. In *Proceedings of the IEEE Conf. on Computer Vision and Pattern Recognition (CVPR)*, 2014. 13
- [16] Adam Coates, Honglak Lee, and Andrew Y. Ng. Stanford stl-10 image dataset. 1, 6, 13
- [17] Alexey Dosovitskiy, Philipp Fischer, Jost Tobias Springenberg, Martin Riedmiller, and Thomas Brox. Discriminative unsupervised feature learning with exemplar convolutional neural networks. *IEEE Transactions on Pattern Analysis and Machine Intelligence*, 38(9):1734–1747, 2016. 4
- [18] Alexey Dosovitskiy, Jost Tobias Springenberg, Martin Riedmiller, and Thomas Brox. Discriminative unsupervised feature learning with convolutional neural networks. In Z. Ghahramani, M. Welling, C. Cortes, N. Lawrence, and K. Q. Weinberger, editors, *Advances in Neural Information Processing Systems*, volume 27. Curran Associates, Inc., 2014. 4
- [19] Debidatta Dwibedi, Yusuf Aytar, Jonathan Tompson, Pierre Sermanet, and Andrew Zisserman. With a little help from my friends: Nearest-neighbor contrastive learning of visual representations. *2021 IEEE/CVF International Conference on Computer Vision (ICCV)*, Oct 2021. 4
- [20] Logan Engstrom, Andrew Ilyas, Shibani Santurkar, Dimitris Tsipras, Brandon Tran, and Aleksander Madry. Adversarial robustness as a prior for learned representations, 2020. 13
- [21] Linus Ericsson, Henry Gouk, and Timothy M. Hospedales. Why do self-supervised models transfer? investigating the impact of invariance on downstream tasks, 2021. 2
- [22] Quentin Garrido, Randall Balestriero, Laurent Najman, and Yann Lecun. Rankme: Assessing the downstream performance of pretrained self-supervised representations by their rank, 2022. 4
- [23] Tom George Grigg, Dan Busbridge, Jason Ramapuram, and Russ Webb. Do self-supervised and supervised methods learn similar visual representations?, 2021. 4

- [24] Jean-Bastien Grill, Florian Strub, Florent Altché, Corentin Tallec, Pierre Richemond, Elena Buchatskaya, Carl Doersch, Bernardo Avila Pires, Zhaohan Guo, Mohammad Gheshlaghi Azar, Bilal Piot, koray kavukcuoglu, Remi Munos, and Michal Valko. Bootstrap your own latent - a new approach to self-supervised learning. In H. Larochelle, M. Ranzato, R. Hadsell, M. F. Balcan, and H. Lin, editors, *Advances in Neural Information Processing Systems*, volume 33, pages 21271–21284. Curran Associates, Inc., 2020. 1, 2, 3, 4, 6, 11
- [25] Kaiming He, Xiangyu Zhang, Shaoqing Ren, and Jian Sun. Deep residual learning for image recognition. In *2016 IEEE Conference on Computer Vision and Pattern Recognition (CVPR)*, pages 770–778, 2016. 4
- [26] Jiabo Huang, Qi Dong, Shaogang Gong, and Xiatian Zhu. Unsupervised deep learning by neighbourhood discovery. In Kamalika Chaudhuri and Ruslan Salakhutdinov, editors, *Proceedings of the 36th International Conference on Machine Learning*, volume 97 of *Proceedings of Machine Learning Research*, pages 2849–2858. PMLR, 09–15 Jun 2019. 4
- [27] Weiran Huang, Mingyang Yi, and Xuyang Zhao. Towards the generalization of contrastive self-supervised learning, 2021. 2
- [28] Li Jing, Pascal Vincent, Yann LeCun, and Yuandong Tian. Understanding dimensional collapse in contrastive self-supervised learning. In *International Conference on Learning Representations*, 2022. 2, 4
- [29] Prannay Khosla, Piotr Teterwak, Chen Wang, Aaron Sarna, Yonglong Tian, Phillip Isola, Aaron Maschinot, Ce Liu, and Dilip Krishnan. Supervised contrastive learning, 2020. 1, 4
- [30] Soroush Abbasi Koohpayegani, Ajinkya Tejankar, and Hamed Pirsiavash. Mean shift for self-supervised learning. *2021 IEEE/CVF International Conference on Computer Vision (ICCV)*, Oct 2021. 4
- [31] Jonathan Krause, Michael Stark, Jia Deng, and Li Fei-Fei. 3d object representations for fine-grained categorization. In *4th International IEEE Workshop on 3D Representation and Recognition (3dRR-13)*, Sydney, Australia, 2013. 13, 14
- [32] Alex Krizhevsky, Vinod Nair, and Geoffrey Hinton. Cifar-10 (canadian institute for advanced research). 1, 6, 13
- [33] Alex Krizhevsky, Vinod Nair, and Geoffrey Hinton. Cifar-100 (canadian institute for advanced research). 1, 6, 13
- [34] S. Maji, J. Kannala, E. Rahtu, M. Blaschko, and A. Vedaldi. Fine-grained visual classification of aircraft. Technical report, 2013. 13, 14
- [35] Maria-Elena Nilsback and Andrew Zisserman. Automated flower classification over a large number of classes. In *Indian Conference on Computer Vision, Graphics and Image Processing*, Dec 2008. 13, 14
- [36] Olga Russakovsky, Jia Deng, Hao Su, Jonathan Krause, Sanjeev Satheesh, Sean Ma, Zhiheng Huang, Andrej Karpathy, Aditya Khosla, Michael Bernstein, Alexander C. Berg, and Li Fei-Fei. ImageNet Large Scale Visual Recognition Challenge. *International Journal of Computer Vision (IJCV)*, 115(3):211–252, 2015. 1, 4, 6
- [37] Ramprasaath R. Selvaraju, Michael Cogswell, Abhishek Das, Ramakrishna Vedantam, Devi Parikh, and Dhruv Batra. Grad-cam: Visual explanations from deep networks via gradient-based localization. *International Journal of Computer Vision*, 128(2):336–359, Oct 2019. 6
- [38] Sahil Singla and Soheil Feizi. Salient imagenet: How to discover spurious features in deep learning?, 2021. 2, 7, 13
- [39] Yonglong Tian, Chen Sun, Ben Poole, Dilip Krishnan, Cordelia Schmid, and Phillip Isola. What makes for good views for contrastive learning? In H. Larochelle, M. Ranzato, R. Hadsell, M. F. Balcan, and H. Lin, editors, *Advances in Neural Information Processing Systems*, volume 33, pages 6827–6839. Curran Associates, Inc., 2020. 4
- [40] Christopher Tosh, Akshay Krishnamurthy, and Daniel Hsu. Contrastive learning, multi-view redundancy, and linear models, 2021. 4
- [41] J. von Kügelgen\*, Y. Sharma\*, L. Gresele\*, W. Brendel, B. Schölkopf, M. Besserve, and F. Locatello. Self-supervised learning with data augmentations provably isolates content from style. In *Advances in Neural Information Processing Systems 34 (NeurIPS 2021)*, Dec. 2021. \*equal contribution. 4
- [42] Zhirong Wu, Yuanjun Xiong, Stella X. Yu, and Dahua Lin. Unsupervised feature learning via non-parametric instance discrimination. In *Proceedings of the IEEE Conference on Computer Vision and Pattern Recognition (CVPR)*, June 2018. 4
- [43] Tete Xiao, Xiaolong Wang, Alexei A Efros, and Trevor Darrell. What should not be contrastive in contrastive learning. In *International Conference on Learning Representations*, 2021. 4
- [44] Asano YM., Rupprecht C., and Vedaldi A. Self-labelling via simultaneous clustering and representation learning. In *International Conference on Learning Representations*, 2020. 4



## A. Appendix

### A.1. Discriminative Features and their Selection

In this section, we study the highly activating features for all samples over the population to find the smaller subsets of features (without using any label information), called *discriminative features*, that are more class-correlated and therefore useful for linear evaluation. We recall  $L_i$  as the set of highly activating features for sample  $i$ . For each highly activating feature  $j$ , the percentage of highly activating samples is denoted by,

$$A_j = \frac{100}{N} \sum_{i=1}^N \mathbb{1}_{j \in L_i} \quad (5)$$

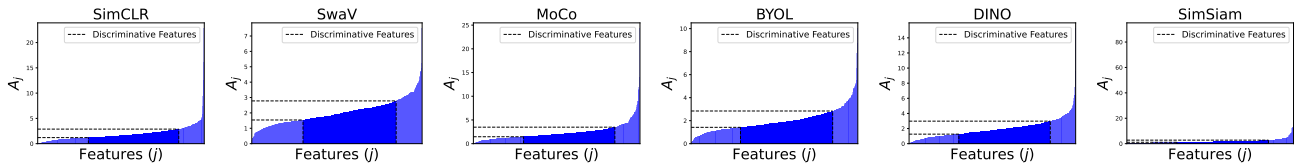


Figure A.1. **Selecting discriminative features:** We plot the percentage of highly activating samples ( $A_j$ ) for each feature in ascending order. We show this for SimCLR [12], SwaV [10], MoCo [13], BYOL [24], DINO [11] and SimSiam [14]. Discriminative features are selected such that they are highly activating for a moderate range of samples, indicating that they may have strong class-correlation, therefore, are useful for downstream classification. Features that are activated for a very large number of samples may not be discriminative as they often encode information common to several classes (e.g. Feature 2021 in Figure 2).

In Figure A.1, we plot  $A_j$  for each feature in the ImageNet-1K representation space of 6 pre-trained state-of-the-art self-supervised models, SimCLR [12], SwaV [10], MoCo [13], BYOL [24], DINO [11] and SimSiam [14]. The x-axis of each plot is ordered by the ascending order of  $A_j$ .

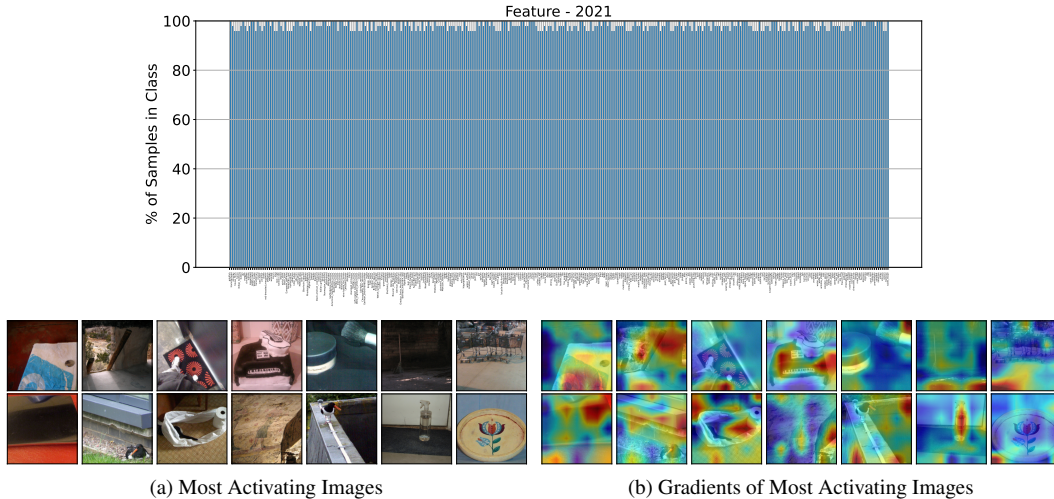
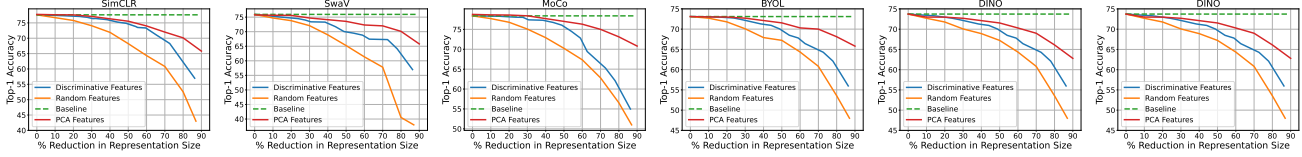


Figure A.2. **Top activating images of feature 2021:** Similar to Figure 2, we plot the top activating samples for feature 2021 in ImageNet-1K trained on SimCLR and group them by classes. We observe that, unlike the features illustrated in Figure 2, this feature activates a large percentage of samples in several classes in the population. If we observe the top activating samples and their gradients (lower panel), we cannot identify a clear physical meaning for this feature. This feature is therefore, not discriminative.

We define three broad categories of highly activating features: (i) Features that are highly activating across a very small fraction of the population, corresponding to the lower tail features in Figure A.1. These features are image-specific and are unlikely to have class-relevance. (ii) Features that are highly activating across a large number of samples in the population i.e, the upper tail features in Figure A.1. Like feature 2021 in Figure A.2), such features are likely to encode very broad and

general characteristics (like texture, color etc.) common to most samples and therefore, are not class-discriminative. The third category includes, (iii) Features that are highly activating across a moderate number of samples in the population (i.e. the middle parts in Figure A.1). These features are most likely to encode unique physical attributes associated with particular classes, similar to those illustrated in the top panel in Figure 2. We refer to this subset of dominant features as *discriminative features* (denoted by the dotted lines in Figure A.1). We emphasize that these discriminative features are selected without the use of any label information.



**Figure A.3. Linear classification accuracy on discriminative features:** We train linear classifiers after selecting subsets of discriminative features of various sizes (middle portion of Figure A.1) and plot their top-1 accuracy for SimCLR, SwaV, MoCo, BYOL, DINO and SimSiam. We compare these results to the baseline, the accuracy on randomly selected features and PCA features of matching sizes. Classifiers trained using discriminative features consistently outperform those of randomly selected features. We can achieve up to 40% reduction in representations size using discriminative features without significantly affecting the top-1 accuracy. Discriminative features also match the performance of PCA features to a certain extent showing that features can be considered as axis-aligned.

We justify the described method of selection in Figure A.3, where we plot the top-1 accuracy of a linear classifier trained on ImageNet-1K using subsets of discriminative features of varying sizes as chosen from Figure A.1 (blue line). We also plot the top-1 accuracy when random subsets of features are selected. We observe that discriminative features perform significantly better compared to randomly selected features. We also observe that we can reduce the representation size up to 40% using the discriminative features, with minimal reduction in performance. In practice, for a given model and dataset, we find that the discriminative features selected between the 30<sup>th</sup> and the 85<sup>th</sup> percentile of  $A$  (as shown in Figure A.1), consistently gives us the best performance.

## A.2. Discriminative Features and Principal Components

In our analysis, we select discriminative features independently and observe their heatmaps and activations across the population. Our analysis is based on the assumption that axis-aligned features can provide meaningful information regarding the quality of the feature representations for self-supervised models. To (partially) validate this assumption, we have conducted a PCA analysis where we select principal components of feature representations and perform linear evaluation on top

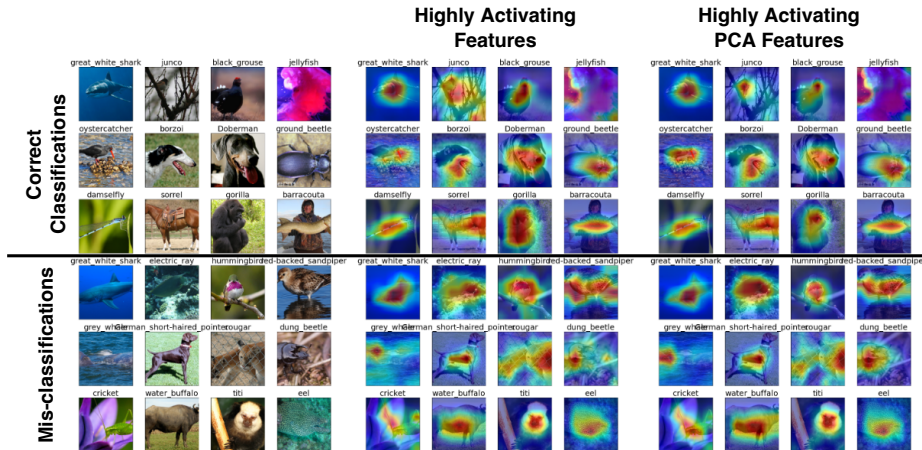


**Figure A.4. Comparing gradient heatmaps of highly activating features and PCA features:** In this figure, we plot the gradient heatmaps of the highly activating features of correct and incorrect classifications on ImageNet-1K trained on SimCLR. We also plot the highly activating PCA features for the same images. We observe that both sets of features activate the same portions of the images meaning that highly activating features can be viewed as axis-aligned.

of them. In Figure A.3, we observe that, until 40% reduction of the representation size, PCA and (axis-aligned) discriminative features perform comparably in terms of the linear classification accuracy while discriminative features significantly outperforms random features across the board. We also plot the gradients of the highly activating PCA features and compare them to highly activating features in the full representation space in Figure A.4. We observe that both sets of features activate the same portions of the images between both correct and incorrect classifications. These results indicate that axis-aligned discriminative features capture a fair amount of information in the feature representations and thus (partially) validating our underlying assumption.

### A.3. Q-Score on Supervised Learning

We note that we select highly activating features and compute Q-Score on self-supervised representations without using any label information. Thus, our study to show correlation between Q-score and classification outcome is non-trivial since self-supervised models learn without labels. Nevertheless, we have included an experiment in Figure A.5, where we analyze Q-score as a predictor of classification outcome (correct vs incorrect) on supervised ResNet-18 (ImageNet-100) and ResNet-50 (ImageNet-1K) representations as well as their robust versions (l2 threat model). Self-supervised representations generally perform better than supervised representations on Q-score indicating that the representational properties we have identified may be mainly prominent in self-supervised learning. We observe that non-robust supervised ResNet shows lower AUROC and AUPRC compared to robust ResNet on both ImageNet-100 and ImageNet-1K setups. This is in line with observations in [20] and [38] that show that robust models provide better axis-alignment of features.

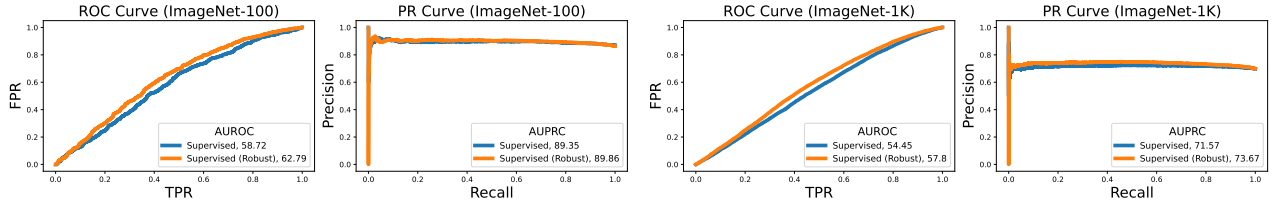


Figure A.5. **Precision-Recall and ROC curves of Q-Score on supervised setups:** In the first two plots, we compute the ROC and PR curves (similar to Figure 4) of Q-score on the representations of a supervised ResNet-18 model and a robust ResNet-18 trained on ImageNet-100. In the last two plots, we show the same for ResNet-50 trained on ImageNet-1K. We observe that robust ResNet performs better for Q-score when used as a predictor for correct or mis-classified representations.

### A.4. Transfer Performance of Q-Score Regularization

In Table A.1, we tabulate the transfer learning performance (linear evaluation) of various unseen datasets [6, 15, 16, 31–35] on 6 self-supervised models trained on ImageNet-1K with and without Q-Score regularization. We use frozen ResNet-50 representations for each transfer dataset (using actual image size) and perform linear evaluation using a classifier. We observe that the average accuracy of unseen datasets improves on all setups, especially on SimCLR, SwaV and MoCo.

Table A.1. **Transfer learning performance of various state-of-the-art self-supervised models trained on ImageNet-1K with and without Q-Score regularization:** We observe that pre-training with Q-Score regularization improves the average transfer accuracy on all self-supervised models.

Transfer Dataset	SimCLR		SwaV		MoCo		BYOL		DINO		SimSiam	
	Baseline	Q-Score Regularized	Baseline	Q-Score Regularized	Baseline	Q-Score Regularized	Baseline	Q-Score Regularized	Baseline	Q-Score Regularized	Baseline	Q-Score Regularized
CIFAR-10	47.30	<b>50.88</b>	56.52	<b>57.07</b>	64.37	<b>65.13</b>	58.83	<b>60.90</b>	<b>58.14</b>	57.42	64.89	<b>65.35</b>
CIFAR-100	27.25	<b>28.56</b>	35.00	<b>36.02</b>	<b>42.22</b>	41.39	35.55	<b>38.06</b>	35.04	<b>35.10</b>	41.66	<b>44.86</b>
STL-10	74.48	<b>77.44</b>	83.65	<b>84.35</b>	87.65	<b>87.68</b>	85.01	<b>85.75</b>	84.53	<b>84.62</b>	87.32	<b>87.95</b>
Aircraft	<b>33.06</b>	32.94	34.08	<b>34.80</b>	26.97	<b>27.30</b>	40.32	<b>42.56</b>	<b>39.54</b>	38.50	25.15	<b>26.75</b>
Flowers	77.24	<b>78.81</b>	<b>83.52</b>	83.29	77.91	<b>77.93</b>	85.59	<b>85.57</b>	85.13	<b>85.66</b>	57.00	<b>61.94</b>
Food	59.11	<b>60.38</b>	64.51	<b>64.77</b>	69.94	<b>71.23</b>	65.59	<b>66.24</b>	59.91	<b>60.22</b>	53.42	<b>54.03</b>
Cars	38.52	<b>41.10</b>	44.59	<b>47.07</b>	32.11	<b>32.30</b>	52.51	<b>54.26</b>	52.23	<b>52.98</b>	<b>33.58</b>	33.01
DTD	59.41	<b>62.39</b>	<b>65.48</b>	64.73	69.68	<b>70.43</b>	<b>66.48</b>	61.95	66.22	<b>67.27</b>	63.45	58.03
Average	52.04	<b>54.06</b>	58.41	<b>59.01</b>	58.85	<b>59.17</b>	61.23	<b>61.91</b>	60.09	<b>60.22</b>	53.30	<b>53.99</b>



Figure A.6. **Highly activating features on unseen datasets:** We visualize the highly activating features discovered on ImageNet-1K classes on unseen datasets like Aircraft [34], Food [6] and Cars [31]. We observe that highly activating features correspond to the same physical attributes as the training data and are core and informative.



Figure A.7. **Comparing correct and mis-classified representations in Flowers dataset:** In these heatmaps, we visualize the highly activating features of several Flowers [35] dataset samples. In the top panel, we display the correct (left) and incorrect (right) classifications of SimCLR (trained on ImageNet-1K) and in the bottom panel, we visualize the same when pre-trained using Q-Score regularization. Similar to the observations in Figure 3, we observe that the regularization enhances highly activating features, thereby leading to an improvement in performance.

In Figure A.6, we visualize the gradient heatmaps of some highly activating features discovered on SimCLR on ImageNet-1K on both ImageNet-1K and unseen datasets, Aircraft [34], Food [6] and Cars [31]. We observe that the physical meaning associated with each feature is consistent between both the training and unseen data. The heatmaps also correspond to informative features, strongly correlated with the ground truth. These gradients indicate that highly activating features are transferable across unseen datasets, which support the improvement we observe in Table A.1.

We also visualize the representations of correct and incorrect classifications of the Flowers [35] dataset in Figure A.7. We use SimCLR pre-trained on ImageNet-1K (top panel) and the same model pre-trained with Q-Score regularization (bottom panel). We observe that the same properties as Figure 3 on ImageNet-1K (train dataset) transfer at test time to Flowers, an unseen dataset. Before regularization, representations, especially the mis-classified ones, do not contain highly activating features. These features get more enhanced after Q-Score regularization leading to improved top-1 accuracy as shown in Table A.1.



## A.5. More Gradient Heatmaps of SimCLR

In Figures A.8, A.9, A.10 and A.11, we plot more heatmaps of highly and lowly activating features of SimCLR for 4 different ImageNet-1K classes. We observe that the highly activating features correspond to unique physical properties that are correlated with the ground truth, whereas, lowly activating features, map to spurious portions that do not contribute to useful information.

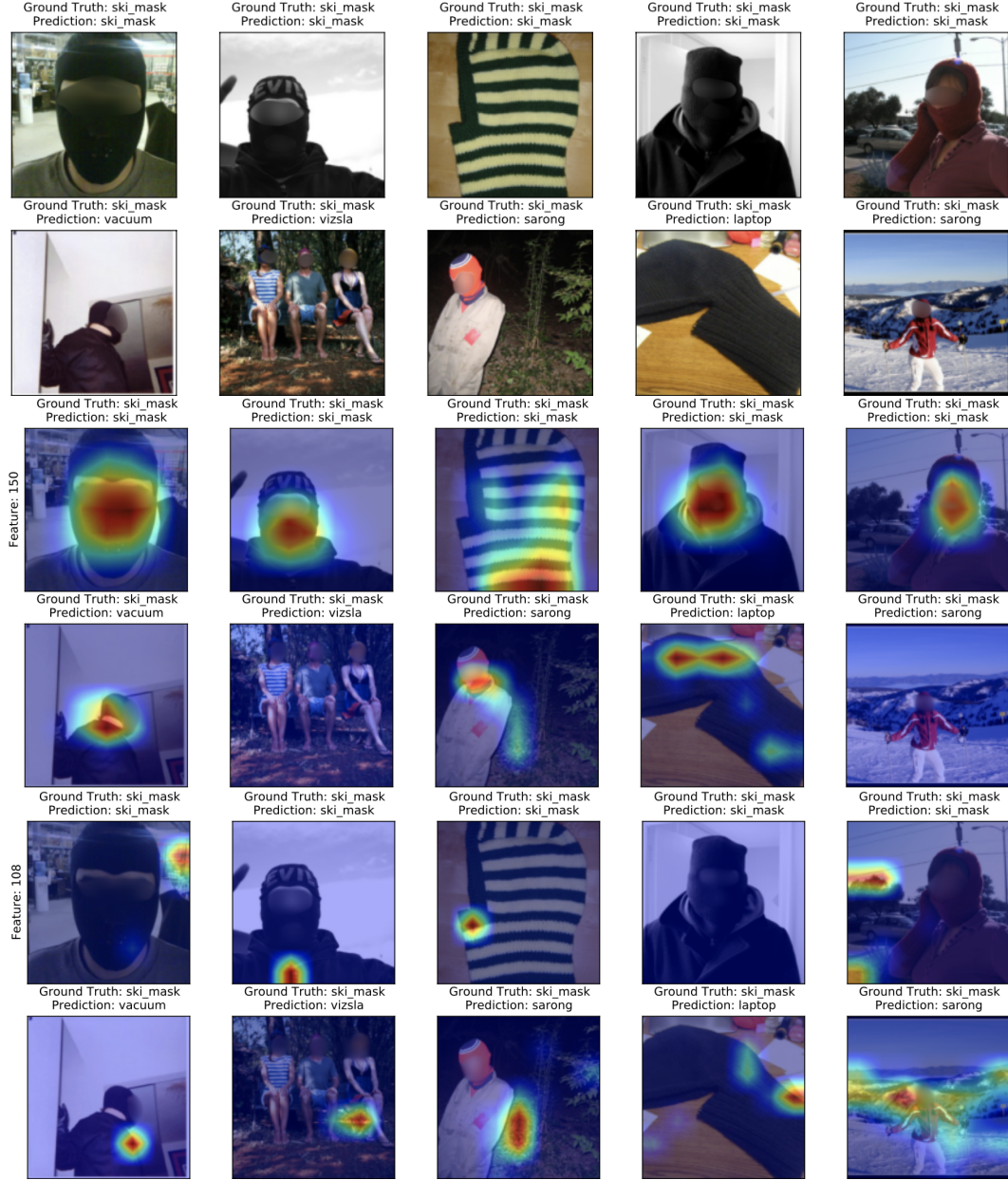


Figure A.8. **Heatmaps of highly activating and lowly activating features of SimCLR (Class - Ski Mask):** We plot the gradient heat maps of the top activating feature (by magnitude) for the given class and a lowly activating feature of the same class. We observe that highly activating features are more correlated with ground truth labels compared to lowly activating features in both correct and incorrect classification. The highly activating feature in correct classifications correspond to a unique physical attribute that may not exist (or be obfuscated) in mis-classified images.

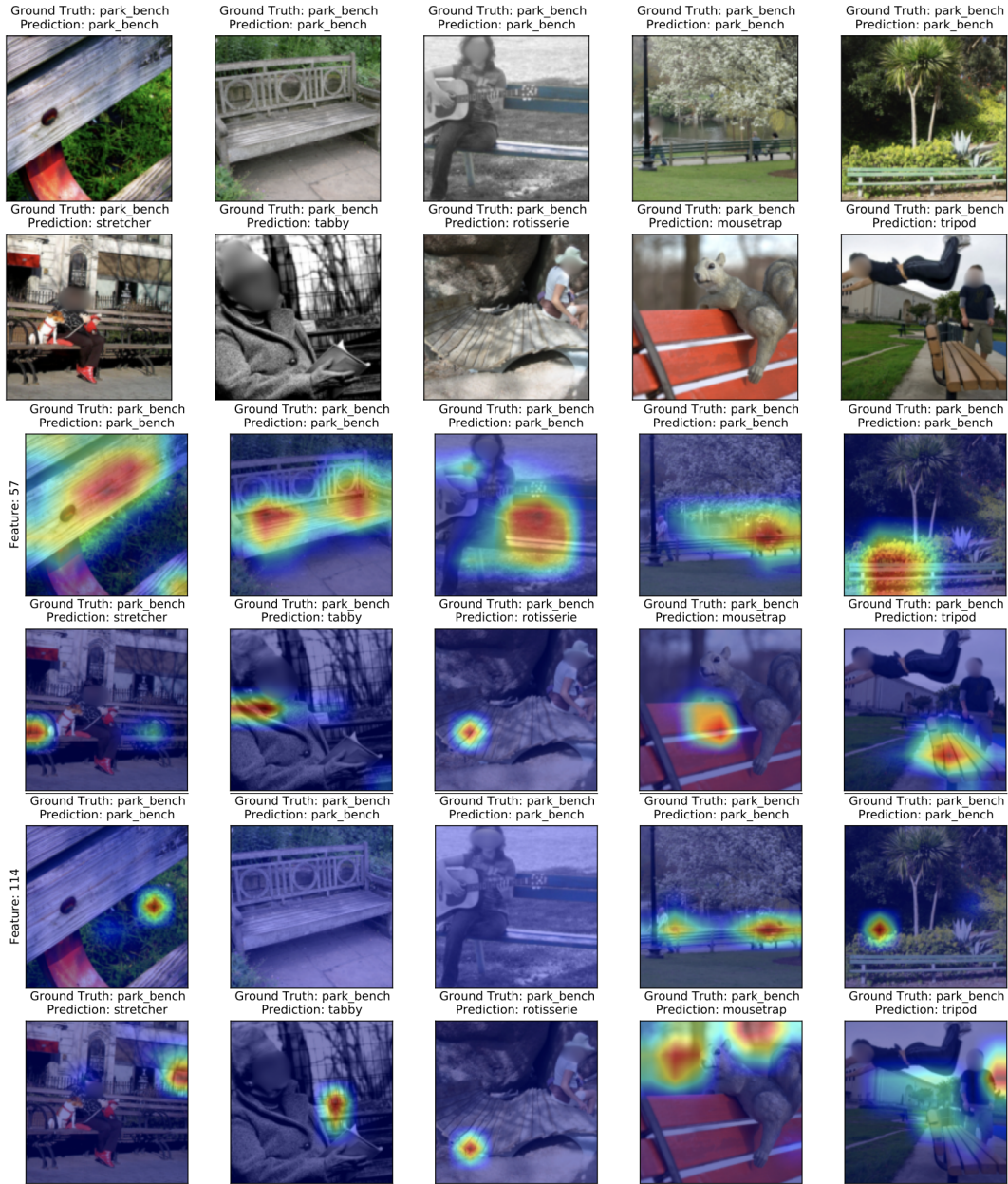


Figure A.9. **Heatmaps of highly activating and lowly activating features of SimCLR (Class - Park Bench):** We plot the gradient heat maps of the top activating feature (by magnitude) for the given class and a lowly activating feature of the same class. We observe that highly activating features are more correlated with ground truth labels compared to lowly activating features in both correct and incorrect classification. The highly activating feature in correct classifications correspond to a unique physical attribute that may not exist (or be obfuscated) in mis-classified images.



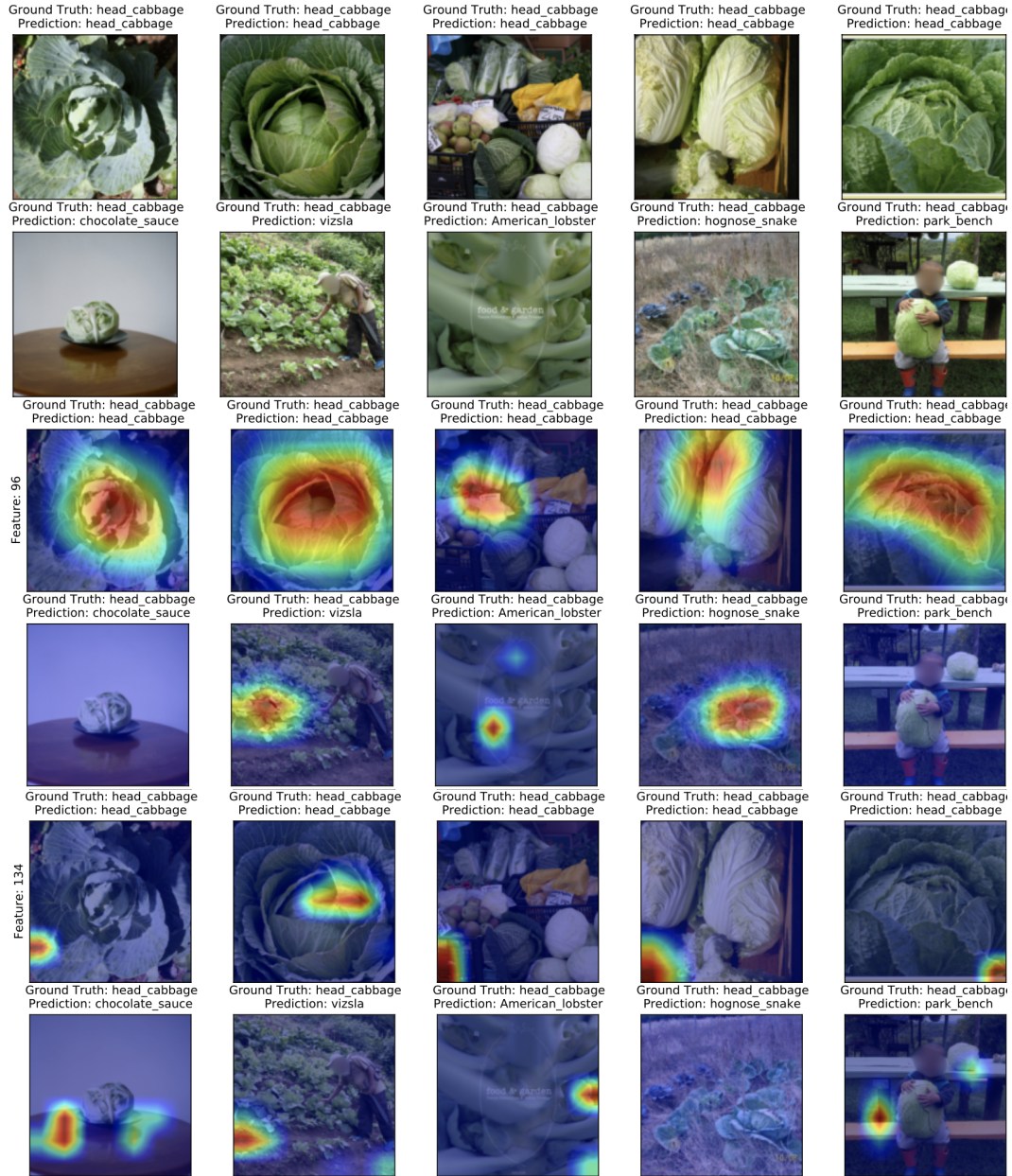


Figure A.10. **Heatmaps of highly activating and lowly activating features of SimCLR (Class - Head Cabbage):** We plot the gradient heat maps of the top activating feature (by magnitude) for the given class and a lowly activating feature of the same class. We observe that highly activating features are more correlated with ground truth labels compared to lowly activating features in both correct and incorrect classification. The highly activating feature in correct classifications correspond to a unique physical attribute that may not exist (or be obfuscated) in mis-classified images.

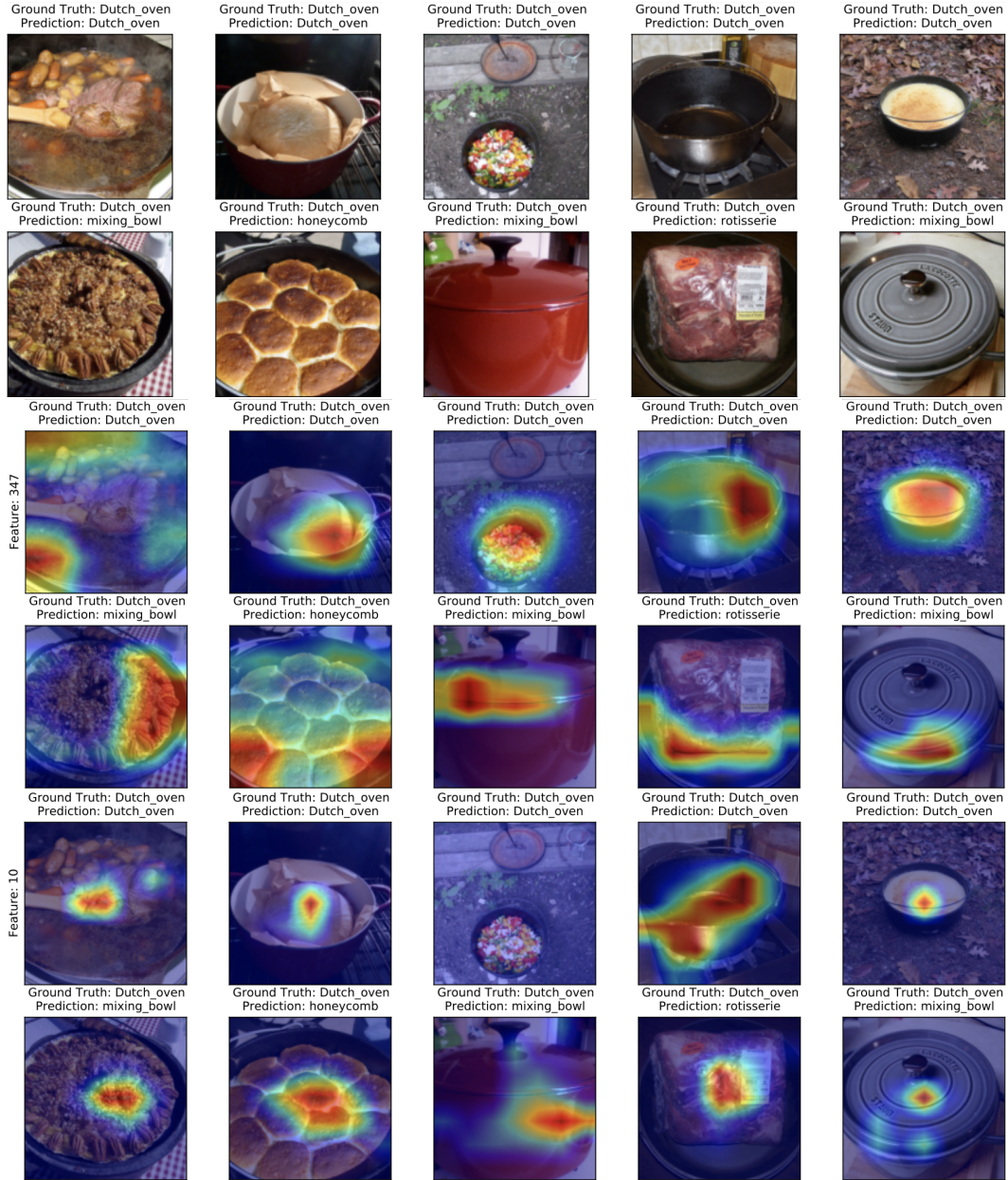


Figure A.11. **Heatmaps of highly activating and lowly activating features of SimCLR (Class - Dutch Oven):** We plot the gradient heat maps of the top activating feature (by magnitude) for the given class and a lowly activating feature of the same class. We observe that highly activating features are more correlated with ground truth labels compared to lowly activating features in both correct and incorrect classification. The highly activating feature in correct classifications correspond to a unique physical attribute that may not exist (or be obfuscated) in mis-classified images.